Deducing the Density of Electronic States at the Fermi Level for Lithiated Carbons Using Combined Electrochemical and Electron Spin Resonance Measurements

Xiaorong Zhou, Lin Zhuang,* and Juntao Lu

Department of Chemistry, Wuhan University, Wuhan 430072, China

Received: February 10, 2003; In Final Form: April 7, 2003

The significance of the band structure for lithiated carbons has been widely recognized, but the band structure is so far not available either theoretically or experimentally for carbons without well-defined structures such as those used in lithium ion batteries. We demonstrate that electron spin resonance can be used to deduce the density of electronic states at the Fermi level, $D(E_F)$, in the course of electrochemical intercalation or deintercalation and to calculate the contribution of band model mechanism to the practical lithiated carbons.

1. Introduction

Carbonaceous materials have been successfully applied in lithium ion batteries for negative electrodes.[1] Massive works have been done worldwide on the mechanism of lithium intercalation into various kinds of carbons,[2] including graphites,[3] hard carbons,[4] mesophase carbons,[5] disordered carbons,[6] carbon nanotubes,[7] etc.[8] Although a fairly sound understanding has been reached of these processes, the quantitative aspect of the structure−property relationship of carbons in this regard has not been well established.[2a] Information is very limited about the quantitative relationship between the properties of different intercalation sites (strictly speaking, the lithium storage processes at some sites may be better called adsorption or covalent bonding, but we shall still use this terminology for simplicity) and their contributions to intercalation. For practical purposes, the performance of lithiated carbon is characterized by the charge (lithium intercalation)/discharge (deintercalation) curve (the charge curve and discharge curve are thermodynamically equivalent except for the first cycle where side reactions occur during charge but not during discharge). Different carbons show charge curves with different features. Some carbons store most intercalated lithium in a narrow potential range close to 0 V (versus metallic lithium in the same solution), while others have their capacitance distributed in a wide range of potential. Graphite is a typical example for the former, while amorphous carbons belong to the latter.[2a] It is obviously significant both practically and academically to be able to understand these features of charge curves more quantitatively.

There have been different models corresponding to different intercalation sites for lithium intercalation into carbons.[9,10] Among these models the band model may be regarded as a well-developed quantitative theory, but its application to carbons without well-defined structures remains an open question. The main feature of the band model is schematically shown in Figure 1. The intercalated lithium is generally assumed to be fully ionized in the host carbon. As lithium ions are intercalated into the carbon from the electrolyte phase, the compensating electrons from the external circuit fill the vacant electronic states of the host starting from the lowest vacant level, resulting in a rise in the Fermi level with respect to a reference level inside the carbon phase. At the same time, the interfacial potential at the carbon/electrolyte interface, $\Delta^C\phi^{sln}$, changes owing to the transfer of lithium ions from the electrolyte to the carbon electrode. The measured electrode potential with respect to a reference electrode (for example, a metallic lithium electrode as shown in Figure 1) corresponds to the difference between the Fermi level of the reference electrode and the Fermi level of the lithiated carbon electrode. The Fermi level of the reference electrode is fixed while the Fermi level of the carbon electrode is rising during charge. The latter is a result of two changes, i.e., the Fermi level rising with respect to a reference level inside the carbon caused by the pouring in of the compensating electrons and the negative shift of the internal potential of carbon caused by the change of $\Delta^C\phi^{sln}$. According to this model, the derivative of the charge curve, $dQ/d\varphi$, for the carbon electrode is closely related to the density of electronic states at the Fermi level, $D(E_F)$.

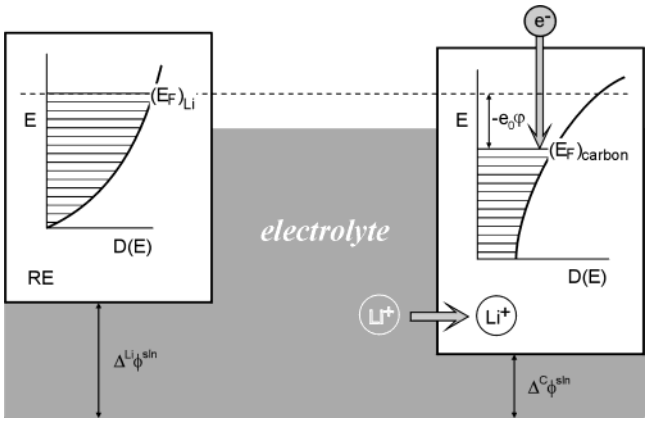

Figure 1. Band model for lithium intercalation into carbons.

There have been theoretical calculations[9,11] as well as experimental works[12] about the band structure of pure graphite and graphite intercalated compounds (GICs). However, the situation of the lithiated carbons of practical technical importance used is more complicated than those theoretically treated and occasionally experimentally studied. First, the mechanism described by the band model is not the only mechanism of lithium intercalation for the complicated structure of the carbons used in lithium batteries. Second, the structure of the carbon powder in real batteries is not well-defined and the band structure for these carbons is not currently available either

* Corresponding author. E-mail: lzhuang@whu.edu.cn.

10.1021/jp034342d CCC: $25.00 © 2003 American Chemical Society
Published on Web 07/03/2003

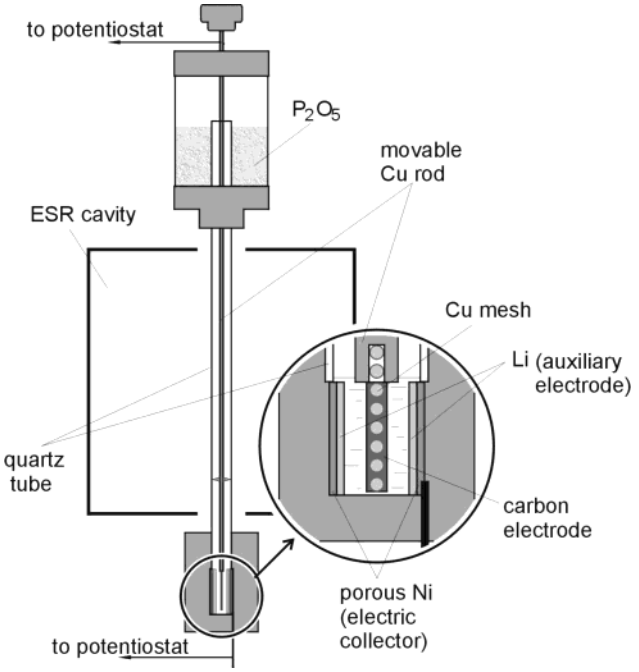

Figure 2. Experimental device for combined ESR−electrochemical measurement for carbon lithiation.

theoretically or experimentally. Third, the assumption of band rigidity in the classical band model may fail in reality. It is therefore highly desirable to determine experimentally the real band structure in the course of lithium intercalation or deintercalation. Gerischer[10] once suggested determination of the $D(E_F)$ for lithiated carbons by measuring the work function, but no successful examples have been found so far.

In this paper, we demonstrate that it is possible to deduce $D(E_F)$ for lithiated carbons by electron spin resonance (ESR) in conjunction with electrochemical measurement. This progress may not only open a new window to get an insight into the structure−property relationship of lithiated carbons but also bear significance for the study of intercalation in general.

2. Experimental Section

The device for ESR−electrochemistry measurements is shown in Figure 2. With a piston mechanism, the test electrode (Teflon bonded carbon powder) could be pushed down to the miniaturized electrolytic cell under the ESR cavity for charge (lithium intercalation) or discharge (deintercalation) and lifted to the cavity center for ESR measurement. The internal atmosphere of the device was kept sufficiently dry by P_2O_5 so that the lithiated carbon electrode could last for 24 h without notable change in ESR signal. The electrode was first fully charged (lithiated) and then discharged. During discharge, the circuit was opened periodically for a few minutes to take the electrode potential under a quasi-equilibrium condition and then the electrode was lifted to the cavity center for ESR measurement. Because the electricity passed during discharge is totally associated with lithium deintercalation, the interference of the charge consumed on the formation of the so-called solid electrolyte interface (SEI) during the first charge process was prevented. In this way, a series of ESR spectra were recorded for various degrees of lithium retention.

ESR measurements were conducted on a JEOL JES-FE1XG (Japan) instrument equipped with a TE_{011} cylindrical cavity and interfaced with a personal computer using a software package developed by the authors. A Mn(II) marker was kept in the cavity as a standard for *g*-factor determination and an indicator for the change in the *Q*-factor of the cavity. l,l-Diphenyl-2-picrylhydrazyl (DPPH, KANTO Chemical Co. Japan) recrystalized in benzene was used as the standard for quantitative determination of the paramagnetic susceptibility. The carbon powder for the test electrode had a sufficiently small particle size to eliminate the distortion of ESR line shape due to limited microwave penetration. To avoid saturation, microwave power was kept low (0.2 mW) in all measurements.

3. Results and Discussion

3.1. Procedure for deducing $D(E_F)$. In our previous work,[13] the principle of deducing $D(E_F)$ for lithiated carbons from ESR measurements was proposed. However, at that time it was not possible to obtain reliable $D(E_F)$ because of two obstacles. One was related to the old cell design that allowed only the first charge process to be observed, and thus the interference of the electricity consumed on SEI formation prevented reliable quantitative data processing. The other was the fact that the recorded ESR signal was not purely due to the electrons at the Fermi level (the Pauli spins) but also due to localized spins (Curie spins). These two problems were overcome in this study. The first one was avoided by using the newly designed ESR cell described in Experimental Section, and the second one was solved by spectral decomposition. Consequently, $D(E_F)$ for practical carbon electrodes can be successfully deduced according to the following procedures.

The $D(E_F)$ of conducting electrons is related to the paramagnetic susceptibility χ_{Pauli} by the following formula:[14]

$$\chi_{Pauli} = \beta^2 D(E_F) \tag{1}$$

where χ_{Pauli} is proportional to the ESR intensity of conducting electrons and β is the Bohr magneton. By comparing with a quantitative DPPH standard, the $D(E_F)$ value can be deduced:

$$D(E_F) = (N_{DPPH} I_{carbon})/(I_{DPPH} kT) \tag{2}$$

where N_{DPPH} is the spin number in the quantitative DPPH standard, I_{carbon} and I_{DPPH} are the ESR intensities for the carbon electrode and the DPPH standard, respectively, k is the Boltzmann constant, and T is the absolute temperature. Equations 1 and 2 are valid to Pauli spins but not to Curie spins. According to our previous variable temperature ESR studies,[15] the ESR signal of lithiated carbons can be split by spectral simulation into two components, corresponding to the Pauli and Curie spins, respectively. In this work, the ESR spectra were first decomposed by simulation and then the Pauli component was used to deduce $D(E_F)$.

According to the above procedures, $D(E_F)$ can be obtained as a function of electrode potential, i.e., the $D(E_F)-\varphi$ relationship. However, the usual way to describe the band structure is $D(E_F)$ as a function of E_F, i.e., $D(E_F) \sim E_F$ or $D(E_F) \sim (E_F - E_F^0)$ relationship, where E_F^0 is a selected Fermi level for reference. Therefore, it is necessary to convert φ to E_F or $(E_F - E_F^0)$ and the conversion will take a few steps as explained below.

As explained in the Introduction, the change of electrode potential, $\Delta\varphi$, due to lithium intercalation consists of two components:

$$\Delta\varphi = \Delta(\Delta^C\phi^{sln}) - \Delta E_F/e_0 \tag{3}$$

where $\Delta(\Delta^C\phi^{sln})$ is the change of the interfacial potential between the electrode (carbon) and the electrolyte solution, ΔE_F is the shift of the Fermi level in the electronic band of carbon,

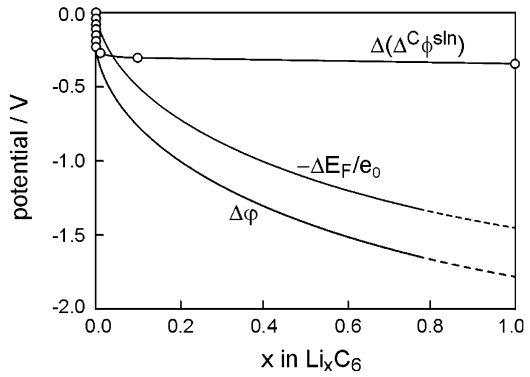

Figure 3. Relative importance of interfacial potential and Fermi level changes. $\Delta\varphi$ is a schematic drawing of the measured electrode potential for real carbon electrodes; $\Delta(\Delta^C\phi^{sln})$ is calculated from eq 4b and $-\Delta E_F/e_0 = \Delta\varphi - \Delta(\Delta^C\phi^{sln})$.

and e_0 represents the absolute value of the charge of an electron. When the electrode is being charged, lithium ions are intercalated into the carbon host from the electrolyte, causing a decrease in the interfacial potential (a negative shift of the internal potential of carbon with respect to the solution); at the same time the compensating electrons from the external circuit are filled in the lowest unoccupied states in the carbon, leading to a rise of the Fermi level with respect to a reference energy level inside the carbon. These two aspects, called the ionic and the electronic factors, respectively,[10] simultaneously drive the electrode potential to the negative.

Neither $\Delta(\Delta^C\phi^{sln})$ nor ΔE_F is experimentally accessible at present. However, if $\Delta(\Delta^C\phi^{sln})$ can be estimated to a good approximation, then ΔE_F can be found through eq 3. The ionic factor $\Delta(\Delta^C\phi^{sln})$ reflects the change of the activity of lithium ions, a_{Li^+}, in the carbon host:

$$\Delta(\Delta^C\phi^{sln}) = -(RT/F)\,\Delta(\ln a_{Li^+}) \qquad (4a)$$

where a_{Li^+} is the product of the concentration x_{Li^+} and the activity coefficient f_{Li^+} of the lithium ions in carbon. As a general rule, the activity coefficient is unity for low concentrations and becomes increasingly larger when concentration increases. The most possible region for f_{Li^+} to increase quickly during the charging process is the potential region close to 0 V (vs Li) where lithiation approaches the maximum. If f_{Li^+} did increase quickly there, the charge curve should bend downward increasingly fast when the electrode potential approaches 0 V. However, it is not generally observed, at least for most lithiated carbons reported. In fact, the electrode potential change with increasing degree of lithiation usually becomes slower when the potential approaches 0 V, the opposite of the prediction of an increasing f_{Li^+}. Therefore, taking f_{Li^+} as unity should be an acceptable approximation. With this approximation, $\Delta(\Delta^C\phi^{sln})$ can be calculated from the change in the concentration of intercalated lithium ions:

$$\Delta(\Delta^C\phi^{sln}) = -(RT/F)\,\Delta(\ln x_{Li^+}) \qquad (4b)$$

Here the concentration x_{Li^+} takes the value of x in the formula Li_xC_6.

Figure 3 analyzes the relative importance of $\Delta(\Delta^C\phi^{sln})$ and ΔE_F. From a practical point of view, it is sufficient to consider a change in x_{Li^+} of 3 orders of magnitude. For practical lithiated carbon electrodes, the measured electrode potential change $\Delta\varphi$ would range from 1.5 to 2.0 V for such a change in x_{Li^+}. According to eq 4b, a change of 3 orders of magnitude in x_{Li^+} corresponds to $\Delta(\Delta^C\phi^{sln}) = 0.18$ V, a minor fraction of the corresponding $\Delta\varphi$. Consequently, $\Delta\varphi$ is mainly governed by ΔE_F in the major potential region of interest. It should be pointed out that x_{Li^+} in eq 4b does not refer to the total amount of intercalated lithium but only to the part describable by the band model. We shall use x_{Pauli} to specify the Pauli spin related intercalation concentration in the text below. To use eq 4b, one has to find out the part of Δx associated with the Pauli spins, Δx_{Pauli}. This can be approximately realized using the $D(E_F)-\varphi$ curve already obtained from ESR measurements as explained below.

The change in x_{Pauli} can be related to $D(E_F)$ and ΔE_F by the following equation:

$$\Delta x_{Pauli} = x_{Pauli(f)} - x_{Pauli(i)} = \int_{E_F(x_i)}^{E_F(x_f)} D(E_F)\,dE_F \qquad (5)$$

where $x_{Pauli(i)}$ and $x_{Pauli(f)}$ are the initial and final lithium ion concentrations related to Pauli spins, respectively. Because ΔE_F accounts for the dominant part (about 90%) of $\Delta\varphi$, for a primary approximation the term $D(E_F)$ in eq 5 (i.e., $D(E_F)$ versus E_F function) can be replaced by the experimentally obtained $D(E_F)$ versus φ function, and dE_F replaced by $d\varphi$. In this way, a curve of $\Delta x_{Pauli}-\Delta\varphi$ can be obtained. In turn, using eqs 4b and 3, $\Delta x_{Pauli}-\Delta(\Delta^C\phi^{sln})$ and $\Delta x_{Pauli}-\Delta E_F$ curves can be deduced. Finally, once a φ value is chosen to correspond to a reference Fermi level E_F^0, the conversion between φ and $(E_F - E_F^0)$ is established. Thus, any function of φ can be numerically converted to corresponding function of $(E_F - E_F^0)$ and vice versa. Also, the relationship of $D(E_F)$ to $(E_F - E_F^0)$ can be successfully deduced.

3.2. $D(E_F)$ for Lithiated Synthetic Graphite. According to the above-described procedures, we processed the ESR data recorded at different potentials in the course of discharge for a lithiated synthetic graphite electrode. The ESR spectra were decomposed to separate the Pauli spins from the Curie spins in the way reported in our previous paper.[15] It was found that at low lithiation levels (i.e., high potentials, such as around 1.5 V, vs metallic Li) the ESR intensity of Curie spins was about 10 times of that of Pauli spins. However, with increasing lithiation level the ESR intensity of Pauli spins rose much faster than that of Curie spins. At the maximum lithiation (near 0 V vs Li), the ESR intensity of Pauli spins was 2 orders of magnitude larger than that at 1.5 V while the Curie spin intensity increased by only a factor of 3.5. As a result, Pauli spins became dominant at higher lithiation levels (low electrode potentials). According to eq 2, $D(E_F) \sim \varphi$ was then obtained. After further processing as described in the preceding section, the $D(E_F)-(E_F - E_F^0)$ curve was obtained as shown in Figure 4 (curve a). For this curve, E_F^0 corresponds to $\varphi = 1.5$ V (vs Li) where $x_{Pauli} = 0.0023$, compared with $x_{Pauli} = 0.24$ at $\varphi = 0$ V. Here, x_{Pauli} stands for the x value associated with Pauli spins in the formula Li_xC_6. The $\Delta(\Delta^C\phi^{sln})$ value corresponding to the electrode potential change from $\varphi = 0$ to 1.5 V is 0.13 V (according to eq 4b).

Also given in Figure 4 are the $D(E_F)$ curves found in the literature for comparison. Curve b is the $D(E_F)$ of the basal plane of highly orientated pyrolytic graphite (OHPG) deduced from the data of differential capacitance measurements.[12a] It is encouraging to see that curves a and b show similar shapes. The difference between these two curves may mainly be attributed to the differences of the samples and the choice of E_F^0. The latter causes a horizontal shift of the curve.

Curve c was converted by the authors from the $x-\Delta E_F$ curve theoretically calculated by Gerouki et al. for single graphene sheets.[9e] They calculated $x-\Delta E_F$ curves for single graphenes

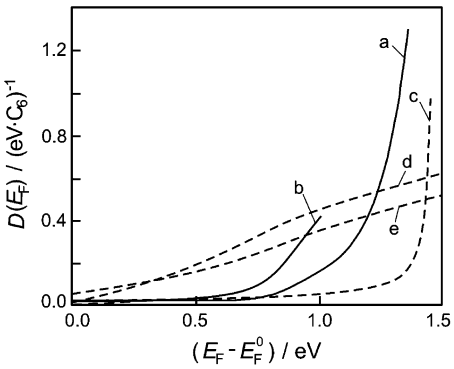

Figure 4. Comparison of $D(E_F)$ curves from different courses. (a) ESR measurement for lithiated synthetic graphite of this work; (b) differential capacitance measurement for HOPG;[12a] (c) converted from the theoretical $x-\Delta E_F$ curve for C_{54} graphene,[9e] amplitude reduced by a factor of 20; (d) theoretical calculation for pristine graphite;[11a] (e) theoretical calculation for boron-substituted graphite.[11b]

ranging from C_{24} to C_{216}. The contribution of the valent electrons at the graphene edges to $D(E_F)$ was considered. They found that the results for larger graphenes (starting from C_{54}) were essentially the same, implying the edge effect decreasing with growing size of the graphene. Curve c in Figure 4 was converted from the original $x-\Delta E_F$ curve for C_{54} by differentiating. Note that the amplitude of curve c is reduced by a factor of 20 to fit the frame. Curve c appears to have a shape similar to those of curves a and b, but $D(E_F)$ increases much faster with E_F for curve c than for curves a and b.

Curves d and e are calculated for pristine graphite[11a] and boron-substituted graphite,[11b] respectively. In calculations for the boron-substituted graphite, the boron atoms were treated exactly the same as carbon atoms except for the number of valent electrons being 3 instead of 4. The two curves appear essentially the same with only a small difference in amplitude, but they are distinctly different from curve c. The prominent difference should stem from the difference in physical models instead of the details of mathematical techniques. The major difference in physical models seems to be the three-dimensional nature for curves d and e in contrast to the two-dimensional nature for curve c. When the five curves in Figure 4 are considered all together, they may be divided into three groups: curve c representing the theoretical result of a two-dimensional model (graphene), curves d and e representing the theoretical results for long range ordered three-dimensional graphite structures, and curves a and b representing the experimental results for real carbon electrodes. Figure 4 reveals that the experimental group happened to be between the other two groups in terms of the increasing rate of $D(E_F)$ with E_F. This might imply that the tested carbon electrodes had intermediate structures: graphenes (possibly with different sizes) piled in order (possibly in different ways) in short ranges. This inference is in line with the existing knowledge about these two electrode materials. It is commonly accepted that there are short range ordered microstructures in the various carbons used in lithium ion batteries. For the HOPG used by Gerischer and coworkers,[12a] the material was reported to show ordered structure within micrometer range under scanning electron microscopy (SEM), but the real ordered range should be smaller than that seen by SEM.

The resemblance of curves a and b is worth some further discussion. It should be noted that the electrodes used, the measurement techniques, and the formulas for data processing were all different for the two curves. The fact that apparently different works produced comparable results must stem from some common points of the two works. In the theoretical aspect, the two works were both based on the band model of conducting electrons for solids; in the experimental aspect, both electrodes seems to consist of short range ordered microstructures. The resemblance of curves a and b should be regarded as a favorable support for both works. Also, it seems reasonable that the two experimental results appeared between the two theoretical extremes, as discussed above.

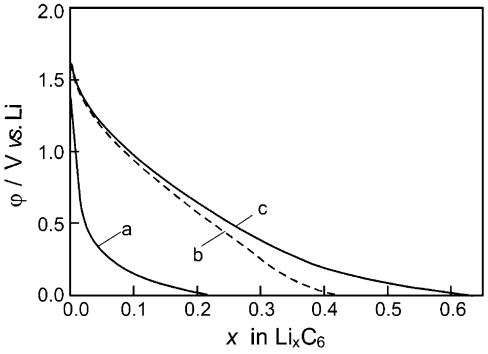

Figure 5. Decomposition of the x vs φ curve for lithium intercalation into synthetic graphite electrode. (a) x_{Pauli}; (b) $x_{non-Pauli}$; (c) x_{total}.

3.3. Estimation of the Contribution of Pauli Sites to Lithiation for Synthetic Graphite. With the experimentally obtained $D(E_F - E_F^0)$ curve, an important new insight into the lithiation of carbons can be gained. Integrating curve a in Figure 4 (using eq 5) and converting $(E_F - E_F^0)$ to φ, one can deduce the contribution of Pauli spin related sites (called the Pauli sites in the text below) to the intercalation as a function of electrode potential, x_{Pauli} versus φ (curve a in Figure 5). Thus, the total intercalation x_{total} (curve c in Figure 5) can be decomposed into x_{Pauli} and $x_{non-Pauli}$ (curve b in Figure 5). The $x_{non-Pauli}$ represents the contribution from all intercalation sites other than the Pauli sites. It is seen that the Pauli contribution becomes increasingly important in the low potential region (below 0.5 V), and at the maximum intercalation ($\varphi = 0$ V) the Pauli contribution accounts for about one-third of the total intercalation for this sample. The other sites for lithium storage may include the adsorption sites on both sides of the graphene sheets in the disordered domains and at the edges of the graphene sheets.[6] It may be noted that the line shape of $x_{Pauli}-\varphi$ resembles the charge curve of graphite; i.e., the most capacity was concentrated within the potential region below 0.5 V. It seems that the Pauli sites belong to the ordered structures and the non-Pauli sites are in the disordered structures.

4. Conclusion

ESR measurement during lithium intercalation or deintercalation has made it possible to deduce the density of electronic states at the Fermi level for different lithiation degrees of carbons without well-defined structures such as those used in lithium ion batteries. This provides unique experimental data to see how the band model works for lithium intercalation into carbons. This technique may also be applicable to intercalation of other ions into carbons and to revealing the band structure for carbons.

Acknowledgment. The authors are grateful to the Natural Science Foundation of China for financial support (NSFC Grant 29873034).

References and Notes

(1) (a) Tirado, J. *Mater. Sci. Eng. R* **2003**, *40*, 103. (b) Tarascan, J.; Armand, M. *Nature* **2001**, *414*, 359. (c) Wakihara, M. *Mater. Sci. Eng. R* **2001**, *33*, 109.

(2) (a) Kinoshita, K.; Zaghib, K. *J. Power Sources* **2002**, *110*, 416. (b) Endo M.; Nishimura, Y.; Takahashi, T.; Takeuchi, K.; Dresselhaus, M. *J. Phys. Chem. Solids* **1996**, *57*, 725. (c) Dahn, J.; Zheng, T.; Liu, Y.; Xue, J. *Science* **1995**, *270*, 590.

(3) (a) Wu, Y.; Jiang, C.; Wan, C.; Holze, R. *Solid State Ionics* **2003**, *156*, 283. (b) Wu, Y.; Jiang, C.; Wan, C.; Holze, R. *J. Power Sources* **2002**, *111*, 329. (c) Wu, Y.; Jiang, C.; Wan, C.; Holze, R. *J. Appl. Electrochem.* **2002**, *32*, 1011. (d) Kim, Y.; Park, S. *J. Electrochem. Soc.* **2001**, *148*, A194. (e) Funabiki, A.; Inaba, M.; Abe, T.; Ogumi, Z. *Carbon* **1999**, *37*, 1591. (f) Menachem, C.; Wang, Y.; Flowers, J.; Peled, E.; Greenbaum, S. *J. Power Sources* **1998**, *76*, 180. (g) Imanishi, N.; Kumai, K.; Kokugan, H.; Takeda, Y.; Yamamoto, O. *Solid State Ionics* **1998**, *107*, 135.

(4) (a) Gautier, S.; Leroux, F.; Frackowiak, E.; Faugere, A.; Rouzaud, J.; Beguin, F. *J. Phys. Chem. A* **2001**, *105*, 5794. (b) Mochida, I.; Ku, C.; Korai, Y. *Carbon* **2001**, *39*, 399. (c) Peled, E.; Eshkenazi, V.; Rosenberg, Y. *J. Power Sources* **1998**, *76*, 153. (d) Liu, Y.; Xue, J.; Zheng, T.; Dahn, J. *Carbon* **1996**, *34*, 193.

(5) (a) Kataoka, H.; Saito, Y.; Omae, O.; Suzuki, J.; Sekine, K.; Toshifumi, K.; Takamura, T. *Electrochem. Solid-State Lett.* **2002**, *1*, A10. (b) Umeda, M.; Dokko, K.; Fujita, Y.; Mohamedi, M.; Uchida, I.; Selman, J. *Electrochim. Acta* **2001**, *47*, 885. (c) Dokko, K.; Fujita, Y.; Mohamedi, M.; Umeda, M.; Uchida I.; Selman J. *Electrochim. Acta* **2001**, *47*, 933. (d) Alcantara, R.; Madrigal, F.; Lavela, P.; Tirado, J.; Mateos, J.; Salazar, C.; Stoyanova, R.; Zhecheva, E. *Carbon* **2000**, *38*, 1031. (e) Lee, S.; Nishizawa, M.; Uchida, I. *Electrochim. Acta* **1999**, *44*, 2379. (f) Tokumitsu, K.; Fujimoto, H.; Mabuchi, A.; Kasuh, T. *Carbon* **1999**, *37*, 1599. (g) Mochida, I.; Ku, C.; Yoon, S.; Korai, Y. *J. Power Sources* **1998**, *75*, 214.

(6) (a) Wang, S.; Yata, S.; Nagano, J.; Okano, Y.; Kinoshita, H.; Kikuta, H.; Yamabe, T. *J. Electrochem. Soc.* **2000**, *147*, 2498. (b) Gong, J.; Wu, H. *Electrochim. Acta* **2000**, *45*, 1753. (c) Wang, S.; Kakumoto, T.; Matsui, H.; Matsumura, Y. *Synth. Met.* **1999**, *103*, 2523. (d) Wang, Z.; Huang, X.; Xue, R.; Chen, L. *Carbon* **1999**, *37*, 685. (e) Gong, J.; Wu, H.; Yang, Q. *Carbon* **1999**, *37*, 1409. (f) Wu, Y.; Wan, C.; Jiang, C.; Fang, S.; Jiang, Y. *Carbon* **1999**, *37*, 1901. (g) Ago, H.; Tanaka, K.; Yamabe, T.; Takegoshi, K.; Terao, T.; Yata, S.; Hato, Y.; Ando, N. *Synth. Met.* **1997**, *89*, 141. (h) Tanaka, K.; Ago, H.; Matsuura, Y.; Kuga, T.; Yamabe, T.; Yata, S.; Hato, Y.; Ando, N. *Synth. Met.* **1997**, *89*, 133. (i) Takami, N.; Satoh, A.; Oguchi, M.; Sasaki, H.; Ohsaki, T. *J. Power Sources* **1997**, *68*, 283. (j) Takami, N.; Satoh, A.; Ohsaki, T.; Kanda, M. *Electrochim. Acta* **1997**, *42*, 2537. (k) Sato, K.; Noguchi, M.; Demachi, A.; Oki, N.; Endo, M. *Science* **1994**, *264*, 556.

(7) (a) Maurin, G.; Henn, F.; Simon, B.; Colomer, J.; Nagy, J. *Nano Lett.* **2001**, *1*, 75. (b) Yang, Z.; Wu, H. *Mater. Chem. Phys.* **2001**, *71*, 7. (c) Claye, A.; Fischer, J.; Huffman, C.; Rinzler, A.; Smalley, R. *J. Electrochem. Soc.* **2000**, *147*, 2845. (d) Claye, A.; Fisher, J.; Metrot, A. *Chem. Phys. Lett*. **2000**, *330*, 61. (e) Wu, G.; Wang, C.; Zhang, X.; Yang, H.; Qi, Z.; He, P.; Li, W. *J. Electrochem. Soc.* **1999**, *146*, 1696.

(8) (a) Skowronski, J.; Knofczynski, K.; Yamada, Y. *Solid State Ionics* **2003**, *157*, 133. (b) Kotina, I.; Lebedev, V.; Ilves, A.; Patsekina, G.; Tuhkonen, L.; Gordeev, S.; Yagovkina, M.; Ekstrom, T. *J. Non-Cryst. Solids* **2002**, *299*, 815. (c) Fukutsuka, T.; Abe, T.; Inaba, M.; Ogumi, Z. *J. Electrochem. Soc.* **2001**, *148*, A1260. (d) Stevens, D.; Dahn, J. *J. Electrochem. Soc.* **2000**, *147*, 4428. (e) Alcantara, R.; Madrigal, F.; Lavela, P.; Tirado, J. *Chem. Mater.* **1999**, *11*, 52.

(9) (a) Madjarova, G.; Yamabe, T. *J. Phys. Chem. B* **2001**, *105*, 2534. (b) Ishikawa, S.; Madjarova, G.; Yamabe, T. *J. Phys. Chem. B* **2001**, *105*, 2534. (c) Ago, H.; Kato, M.; Yahara, K.; Yoshizawa, K.; Tanaka, K.; Yamabe, T. *J. Electrochem. Soc.* **1999**, *146*, 1262. (d) Yamabe, T.; Tanaka, K.; Ago, H.; Yoshizawa, K.; Yata, S. *Synth. Met.* **1997**, *86*, 2411. (e) Gerouki, A.; Goldner, M.; Goldner, R.; Haas, T.; Liu, T.; Slaven, S. *J. Electrochem. Soc.* **1996**, *143*, L262.

(10) Gerischer, H.; Decker, F.; Scrosati, B. *J. Electrochem. Soc.* **1994**, *141*, 2297.

(11) (a) Tatar, R.; Rabii, S. *Phys. Rev. B* **1982**, *25*, 4126. (b) Dahn, J.; Reimers, J.; Sleigh, A.; Tiedje, T. *Phys. Rev. B* **1992**, *45*, 3773. (c) Eberhardt, W.; McGovern, I.; Plummer, E.; Fisher, J. *Phys. Rev. Lett.* **1980**, *44*, 200. (d) Holzwarth, N.; Rabii, S.; Girifalco, L. *Phys. Rev. B* **1978**, *18*, 5190. (e) Holzwarth, N.; Girifalco, L.; Rabii, S. *Phys. Rev. B* **1978**, *18*, 5206. (f) McClure, J. *Phys. Rev.* **1957**, *108*, 612. (g) Elliott, R. *Phys. Rev.* **1954**, *96*, 266. (h) Wallace, P. *Phys. Rev.* **1947**, *71*, 622.

(12) (a) Gerischer, H.; McIntyre, R.; Scherson, D.; Storck, W. *J. Phys. Chem.* **1987**, *91*, 1930. (b) Delhaes, P.; Rouillon, J.; Manceau, J. *J. Phys. (Paris)* **1976**, *37*, L127.

(13) Zhuang, L.; Lu, J.; Ai, X.; Yang, H. *J. Electroanal. Chem.* **1995**, *397*, 315.

(14) Kittel, C. *Introduction to Solid State Physics*, 7th ed.; John Wiley & Sons: New York, 1996; Chapter 14.

(15) Du, Z.; Zhuang, L.; Lu, J. *Chin. Chem. Lett.* **2001**, *12*, 163.